Arch. Metall. Mater. **63** (2018), 2, 875-882

DOI: 10.24425/122417

K. TIAN*,**#, B. TIAN*,**#, A.A. VOLINSKY***, Y. ZHANG*,**, Y. LIU*,**, Y. DU****

Y ADDITION EFFECTS ON HOT DEFORMATION BEHAVIOR OF Cu-Zr ALLOYS WITH HIGH Zr CONTENT

Isothermal hot compression experiments were carried out using the Gleeble-1500D thermal mechanical simulator. The flow stress of the Cu-1%Zr and Cu-1%Zr-0.15%Y alloys was studied at hot deformation temperature of 550°C, 650°C, 750°C, 850°C, 900°C and the strain rate of 0.001 s^{-1}, 0.01 s^{-1}, 0.1 s^{-1}, 1 s^{-1}, 10 s^{-1}. Hot deformation activation energy and constitutive equations for two kinds of alloys with and without yttrium addition were obtained by correlating the flow stress, strain rate and deformation temperature. The reasons for the change of hot deformation activation energy of the two alloys were analyzed. Dynamic recrystallization microstructure evolution for the two kinds of alloys during hot compression deformation was analyzed by optical and transmission electron microscopy. Cu-1%Zr and Cu-1%Zr-0.15%Y alloys exhibit similar behavior of hot compression deformation. Typical dynamic recovery occurs during the 550-750°C deformation temperature, while dynamic recrystallization (DRX) occurs during the 850-900°C deformation temperature. High Zr content and the addition of Y significantly improved Cu-1%Zr alloy hot deformation activation energy. Compared with hot deformation activation energy of pure copper, hot deformation activation energy of the Cu-1%Zr and Cu-1%Zr-0.15%Y alloys is increased by 54% and 81%, respectively. Compared with hot deformation activation energy of the Cu-1%Zr alloy, it increased by 18% with the addition of Y. The addition of yttrium refines grain, advances the dynamic recrystallization critical strain point and improves dynamic recrystallization.

Keywords: Cu-1%Zr alloy, high Zr content, yttrium, hot deformation activation energy, dynamic recrystallization

1. Introduction

Copper alloys with high strength and electrical conductivity, and adequate thermal conductivity, are widely used in electrical switching contact bridges [1], crystallizer lining of continuous casting systems, electric cars, electric locomotive overhead wires [2], high pulse magnetic field conductors [3] and electrified high-speed railway contacts [4]. Copper alloys with excellent performance have been utilized, including medium conductivity Cu-Fe-P alloys [5,6], high strength and medium conductivity Cu-Ni-Si alloys [7] and high strength and high conductivity Cu-Cr-Zr alloys [8]. In order to improve comprehensive performance of copper alloys, researchers usually add some trace elements or micro-alloying elements. Some examples include Si with deoxidation, purification and liquidity of copper alloy melts [9], while adding a small amount of Sn can inhibit the aging process of Cr in precipitation [10]. Adding appropriate amounts of Mg can delay precipitation phase growth and reduce surrounding cohesion stress [11]. These studies mainly concentrated on the melting process or comprehensive performance and microstructure after cold deformation and aging. However, plastic deformation and microstructure evolution due trace rare earth elements addition have not been adequately investigated for the Cu-Zr alloy during hot deformation. According to the Cu-Zr alloy binary phase diagram, Zr maximum solid solubility in Cu is 0.15% at 966°C. Zr content near maximum solid solubility in the Cu-Zr alloy was studied by several researchers. Yu et al. [12] studied precipitation sequence of the Cu-Cr-Zr-Mg alloy during early aging stage , where Zr content was 0.1%, Wang et al. [13] studied the effect of direct current pulses on mechanical and electrical properties of aged Cu-Cr-Zr alloys, and Zr content in the alloy was 0.3%. L. Jiang [14] studied pre-deformation and aging characteristics of the Cu-Te-Zr alloy with Zr content of 0.2%. Zhang et al. [15] studied processing maps for the Cu-Cr-Zr-Y alloy hot deformation behavior, where Zr content was 0.1%. In this study Zr content of the Cu-Zr alloy was selected at 1%, which is far higher than its maximum solid solubility. Excess Zr is supposed to form an excess phase. Excess phase enhancement effects occur after solution and aging treatments. When the crystal is deformed, it is changed into the interface strengthening effect to obtain high strength and high conductivity of copper alloys. It is mainly used in conductive structural materials operating at high temperature conditions, such as continuous casting machine mold lining, separation ring, coal-fired power plant burner nozzle and spot welding electrode. Therefore, the effects of Y trace rare earth element addition on hot deformation behavior of Cu-1%Zr alloy with high Zr content were investigated.

* HENAN UNIVERSITY OF SCIENCE AND TECHNOLOGY, SCHOOL OF MATERIALS SCIENCE AND ENGINEERING, LUOYANG 471023, CHINA
** COLLABORATIVE INNOVATION CENTER OF NONFERROUS METALS, HENAN PROVINCE, LUOYANG 471023, CHINA
*** UNIVERSITY OF SOUTH FLORIDA, DEPARTMENT OF MECHANICAL ENGINEERING, TAMPA FL 33620, USA
**** INSTITUTE OF MICROELECTRONICS OF CHINESE ACADEMY OF SCIENCES, SUZHOU 215347, CHINA

\# Corresponding authors: tianka123@163.com, bhtian007@163.com

2. Experimental details

The experimental alloy was melted in a vacuum induction furnace under argon atmosphere by using 99.95 wt.% (mass fraction) standard cathode copper Cu-CATH-2, Zr block with 99.5% purity and rare earth Y metal block with 99.5% purity, which were cast into a low carbon steel mold with ϕ80 mm × 150 mm dimensions. The Cu-1%Zr and Cu-1%Zr-0.15%Y alloys were extruded into ϕ33 mm diameter rod using the XJ-500 extrusion machine. The extruded rods were solution treated at 900°C for 1 hour, followed by water quenching. The specimens were processed into ϕ8 mm × 12 mm cylinders. The isothermal compression experiment was performed using the Gleeble-1500D thermal simulator system. The test parameters were as following: compression temperature of 550°C, 650°C, 750°C, 850°C, 900°C and the strain rate of 0.001 s^{-1}, 0.01 s^{-1}, 0.1 s^{-1}, 1 s^{-1} and 10 s^{-1}, respectively. Total compression deformation was 55%. The heating rate was 10°C/s with 6 min holding time. After hot compression, the specimen was water quenched to room temperature in order to preserve elevated temperature deformed microstructure.

3. Results and analysis

3.1. The true stress-true strain curves

The true stress-true strain curves of the Cu-1%Zr and Cu-1%Zr-0.15%Y alloys during hot compression deformation are shown in Fig. 1. The flow stress decreased with the deformation temperature at a given stain rate, while it increased with the strain rate at the same deformation temperature. This indicates that the flow stress of the alloy is significantly influenced by the strain rate and deformation temperature. Typical characteristics of dynamic recovery occurs at 550-750°C, while dynamic recrystallization occurs at 850-900°C deformation temperature. At the initial stage of thermal deformation, the flow stress of the alloy sharply increases due to increasing true strain. With increasing true strain, the flow stress increase slows down, eventually becoming constant stress or even declining, which indicates that the alloy has relatively complex thermal deformation mechanism. During the hot deformation process, grains deformation and elongation lead to lattice distortions. Dislocation density is sharply raised, and dislocations move in the process of mutual accumulation and cutting, forming networks like dislocation winding structures, producing the hardening phenomenon, as shown in Fig. 2a. Under lower deformation temperature, the internal stress of the deformed alloy accumulates to a certain degree, and dynamic recovery happens resulting in lower dislocation density, and the true stress increases slowly with true strain, as seen in Fig. 1c at 550°C. Under higher deformation temperature, dislocations at the sub-grain boundaries, formed during the recovery process, gradually transfer or merge through dissociation, dismantling and dislocation slip. From the dislocation of the high energy state to the low energy state, the redistribution of the dislocation wall will be divided into a number of sub-grains, as seen

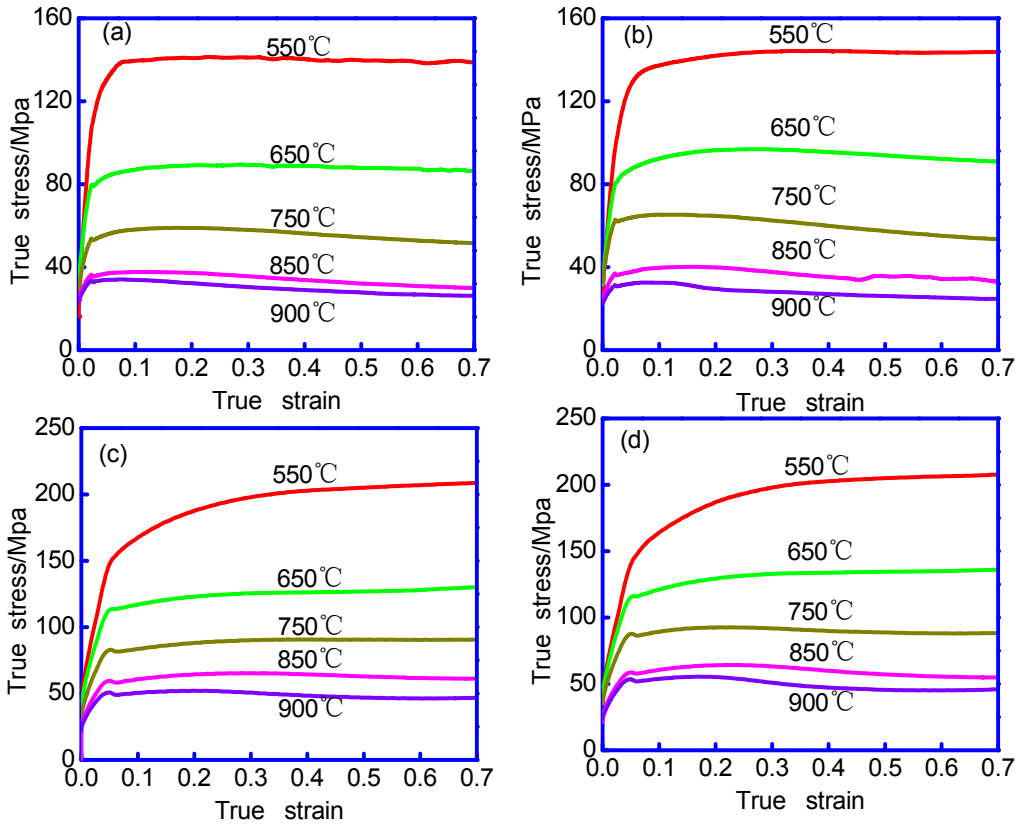

Fig. 1. True stress-true strain curves of Cu-1%Zr(a, c) and Cu-1%Zr-0.15%Y(b, d) alloys deformed at different temperature and strain rate: (a) $\dot{\varepsilon}$ = 0.001 s^{-1}; (b) $\dot{\varepsilon}$ = 0.001 s^{-1}; (c) $\dot{\varepsilon}$ = 0.1 s^{-1}; (d) $\dot{\varepsilon}$ = 0.1 s^{-1}

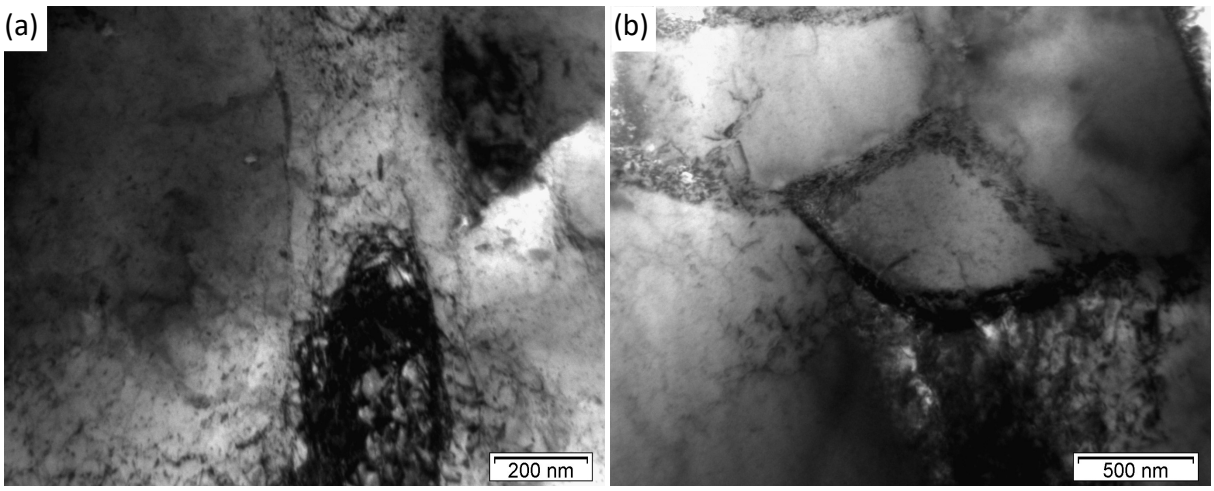

Fig. 2. TEM micrographs of the Cu-1%Zr alloy deformed at 0.1 s^{-1} strain rate and different temperature: (a) 550°C; (b) 850°C

in Fig. 2b. Adjacent sub-grain boundaries gradually disappear and sub-grains merge forming large angle grain boundaries, which contribute to forming recrystallization nuclei. Recrystallization nuclei boundaries move towards the distorted area. The alloy softening rate is greater than the strain hardening rate, and the true stress decreases, as seen in Fig. 1d at 850°C. As the deformation hardening rate becomes equivalent to the dynamic recovery and dynamic recrystallization rates, the true stress-true strain curves tend to be steady, as seen in Fig. 1a at 650°C. The main reason for the above changes is competition between dynamic thermal processing of strain hardening and dynamic softening of recovery and recrystallization occurring simultaneously.

Based on the true stress-true strain curves of the two alloys, dynamic recrystallization of the Cu-1%Zr-0.15%Y alloy is easier than the Cu-1%Zr alloy, as seen in Fig. 1a and Fig. 1b. At 650°C deformation temperature with the 0.001 s^{-1} strain rate, the true stress-true strain curve of the Cu-1%Zr alloy has typical characteristics of dynamic recovery, while Cu-1%Zr-0.15%Y exhibits obvious characteristics of dynamic recrystallization. The stacking fault energy of Cu substrate is relatively lower [16], and the addition of Y increases the extended dislocation width. It is difficult to make the cross slip and edge dislocation climb change to dynamic recovery. Therefore, the tendency of dynamic recrystallization is obvious. The Y plays a role in grain refinement. Finer grains cause harder deformation ability and higher energy storage. The number of recrystallization nuclei formed per unit volume will increase. At the same time smaller grains increase the grain boundary area, which can provide more nucleation sites for easier dynamic recrystallization.

3.2. Effect of Y addition on Cu-1%Zr alloy deformation activation energy

Hot plastic deformation at elevated temperature of metallic materials is similar to high temperature creep, both of which are heat activated processes. The flow stress depends on the deformation temperature T and the strain rate $\dot{\varepsilon}$. C.M. Sellars and C. Bruni according to Arrhenius relationship, proposed to use hyperbolic sine form to describe the relationship among σ, $\dot{\varepsilon}$ and T [17-19]:

$$\dot{\varepsilon} = AF(\sigma)\exp\left[-\frac{Q}{RT}\right] \tag{1}$$

The formula (1) is a function of stress, and there are three different forms under different bars [20]:

$$\dot{\varepsilon} = A_1\sigma^{n_1}\exp\left[-\frac{Q}{RT}\right] \qquad (\alpha\sigma < 0.8) \tag{2}$$

$$\dot{\varepsilon} = A_2\exp(\beta\sigma)\exp\left[-\frac{Q}{RT}\right] \quad (\alpha\sigma > 1.2) \tag{3}$$

$$\dot{\varepsilon} = A\left[\sinh(\alpha\sigma)\right]^n\exp\left[-\frac{Q}{RT}\right] \tag{4}$$

Here, A_1, A_2, A are a structural factor, n is the stress exponent, α is the stress level parameter, Q is the hot deformation activation energy, R is the molar gas constant. Equations mentioned above can be rewritten using Zener-Holomon Z-parameter that is defined as follows [21]:

$$Z = \dot{\varepsilon}\exp(Q/RT) \tag{5}$$

The formulas (2), (3) and (4) are derived separately.

$$\ln\dot{\varepsilon} = \ln A_1 - \frac{Q}{RT} + n_1\ln\sigma \tag{6}$$

$$\ln\dot{\varepsilon} = \ln A_2 - \frac{Q}{RT} + \beta\sigma \tag{7}$$

$$\ln Z = \ln A + n\ln[\sinh(\alpha\sigma)] \tag{8}$$

Subsequently, ln$\dot{\varepsilon}$ and lns are used as coordinate axes, and ln$\dot{\varepsilon}$ and s are used as coordinate axes for plotting, as shown in Fig. 3a and Fig. 3b. Using the least square method, n_1 takes the

average value of the three slopes of the line $\ln\dot{\varepsilon} - \ln\sigma$ where the peak stress are minimal, the temperature corresponding to them are 750°C, 850°C and 900°C. Simultaneously, β takes the average value of the three slopes with the maximum peak stress of the line $\ln\dot{\varepsilon} - \sigma$, the temperature corresponding to them are 550°C, 650°C and 750°C. Then $\alpha = \dfrac{\beta}{n_1} = 0.012$. One can take natural logarithms of both sides of the equation (4) to express the following Q factor:

$$Q = R\frac{\partial \ln[\sinh(\alpha\sigma)]}{\partial(1/T)}\bigg|_{\dot{\varepsilon}} \cdot \frac{\partial \ln\dot{\varepsilon}}{\partial \ln[\sinh(\alpha\sigma)]}\bigg|_{T} = nRK \qquad (9)$$

According to the peak stress, the corresponding temperature and strain rate, the $\dot{\varepsilon}$ and $\ln[\sinh(\alpha\sigma)] - 1/T$ curves are plotted respectively. The results are shown in Fig. 3c and Fig. 3d. The mean value of the five slopes of the line $\ln\dot{\varepsilon} - \ln[\sinh(\alpha\sigma)]$ is represented by n, the mean value of the five slopes of the line $\ln[\sinh(\alpha\sigma)] - 1/T$ is represented by K, get $n = 8.70$, $K = 5.24$. Therefore, $Q = nRK = 379$ kJ/mol. When the $\dot{\varepsilon}$, T and Q are fixed, draw the line $\ln Z - \ln[\sinh(\alpha\sigma)]$, as shown in Fig. 3e. Intercept $\ln A = 39.63$, $A = 1.63\times10^{17}$. Therefore, the constitutive equation for hot deformation of the Cu-1%Zr-0.15%Y alloy is expressed as:

$$\dot{\varepsilon} = 1.63\times10^{17}\left[\sinh\left(0.012\sigma\right)\right]^{8.7}\exp\left(-\frac{379}{RT}\right) \qquad (10)$$

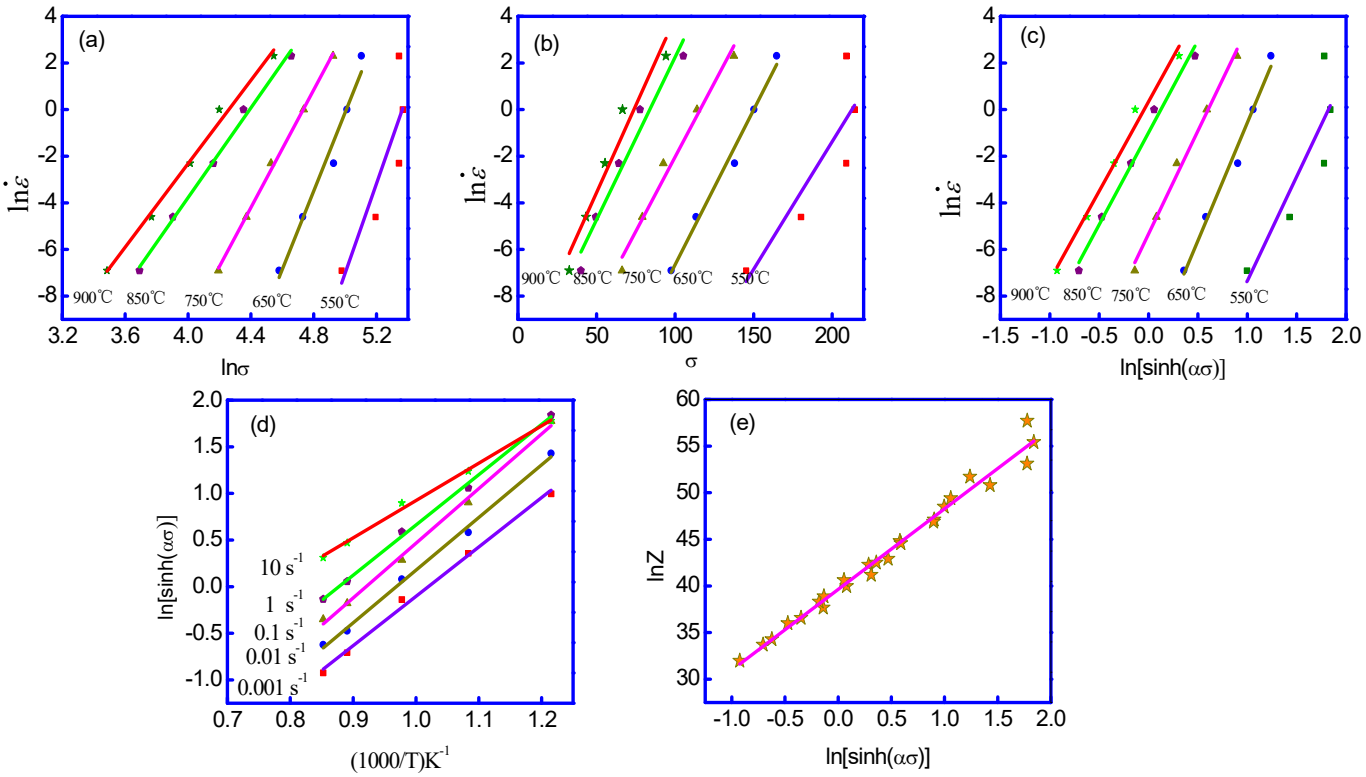

Fig. 3. Relationships between the peak flow stress, deformation temperature and strain rate for the Cu-1%Zr-0.15%Y alloy: (a) $\ln\dot{\varepsilon} - \ln\sigma$; (b) $\ln\dot{\varepsilon} - \sigma$; (c) $\ln\dot{\varepsilon} - \ln[\sinh(\alpha\sigma)]$; (d) $\ln[\sinh(\alpha\sigma)] - 1/T$; (e) $\ln Z - \ln[\sinh(\alpha\sigma)]$

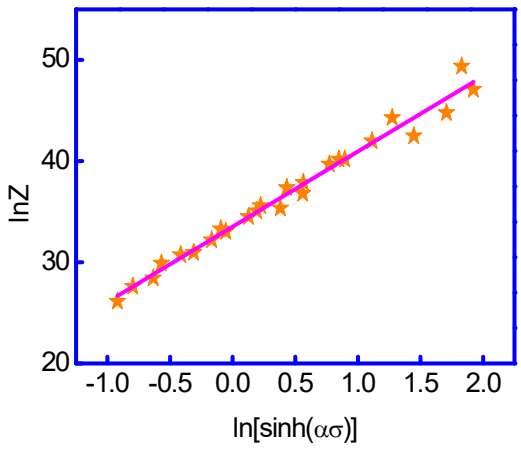

Fig. 4. Relationship between $\ln Z$ and $\ln[\sinh(\alpha\sigma)]$ for Cu-1%Zr alloy

Similarly, the parameters for Cu-1%Zr alloy are: $A = 3.61 \times 10^{14}$, $n = 7.50$, $\alpha = 0.011$, $Q = 322$ kJ/mol. The $\ln Z$ and $\ln[\sinh(\alpha\sigma)]$ relation for Cu-1%Zr alloy is shown in Fig. 4. The fitting coefficient is 0.98, and the coincidence degree is very high. Therefore, the constitutive equation for the Cu-1%Zr alloy can be expressed as:

$$\dot{\varepsilon} = 3.61\times10^{14}\left[\sinh\left(0.011\sigma\right)\right]^{7.5}\exp\left(-\frac{322}{RT}\right) \qquad (11)$$

Hot deformation activation energy is an important parameter to measure the degree of difficulty to plastic deformation of a metal. Hot deformation activation energy of the Cu-1%Zr alloy is 322 kJ/mol, while hot deformation activation energy of the Cu-1%Zr-0.15%Y alloy is 379 kJ/mol and the deformation activation

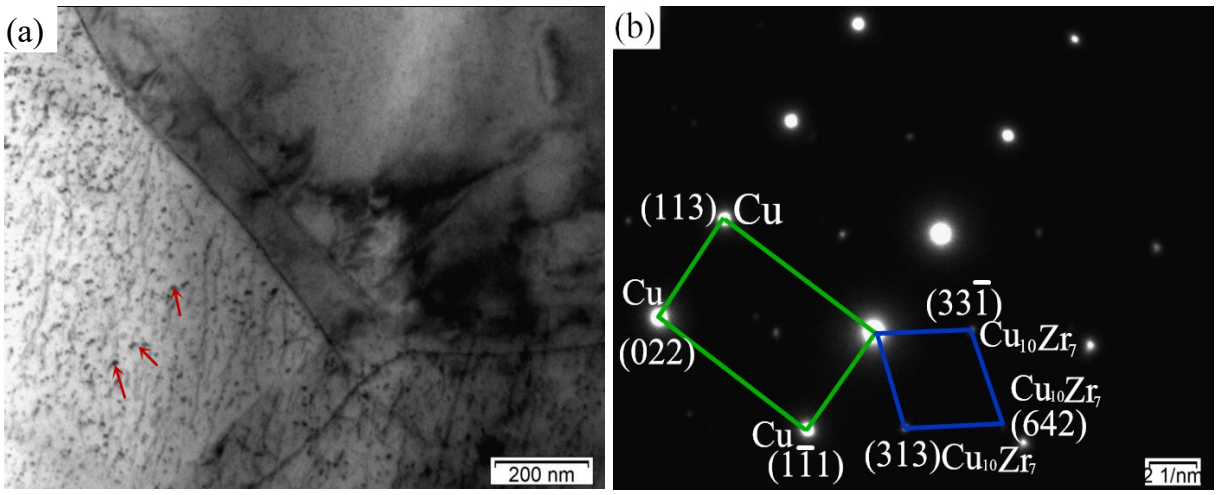

Fig. 5. (a) TEM micrographs of the Cu-1%Zr alloy deformed at 0.1 s^{-1} strain rate and 850°C; (b) selected area diffraction pattern from (a)

energy of pure copper is 209 kJ/mol [22]. Compared with hot deformation activation energy of pure copper, hot deformation activation energy of the Cu-1%Zr and Cu-1%Zr-0.15%Y alloys is increased by 54% and 81%, respectively. The reason for this is that Zr addition had solid solution strengthening effect, impeding dislocation slip and climb. Zr maximum solid solubility in Cu is 0.15% at 966°C, and there are many precipitates in the Cu matrix, which have an effect on dislocation pinning, as shown in Fig. 5a. Selected area diffraction patterns obtained from the precipitates are shown in Fig. 5b. It can be seen that the precipitates identified in the present study were $Cu_{10}Zr_7$. According to the PDF card 47-1028 [23], the lattice parameters for $Cu_{10}Zr_7$ phase are a = 1.2675 nm, b = 0.9313 nm, c = 0.9347 nm.

Comparing hot activation energy of the Cu-1%Zr and Cu-1%Zr-0.15%Y alloys, it increased by 18% with the addition of Y. On the one hand, the atomic radius of Cu is 0.128 nm, while the atomic radius of Y is 0.180 nm, which is about 41% difference. Therefore, Y has low solid solubility in Cu, and the solid solution strengthening effect is obvious. On the other hand, Y has an effect of removing impurities and deoxygenating, as Y with impurities in copper forms refractory compounds. Hot large deformation increases the number of dislocations. Hot deformation at the same conditions increases the amount of stored energy in the matrix, providing additional driving force for dynamic recovery and dynamic recrystallization.

3.3. Effect of Y addition on Cu-1%Zr alloy microstructure

Fig. 6 shows microstructure of the Cu-Zr and Cu-1%Zr-0.15%Y alloys solution treated at 900°C for 1 h, where Y addition can evidently refine the grain size. Optical micrographs of the Cu-1%Zr and Cu-1%Zr-0.15%Y alloys deformed at 0.1 s^{-1} strain rate and different temperatures are shown in Fig. 7. Fig. 7a and Fig. 7c are Cu-1%Zr structures. Fig. 7b and Fig. 7d are Cu-1%Zr-0.15%Y structures. When the deformation temperature is 550°C with the 0.1 s^{-1} strain rate, large grains are elongated and there are no dynamic recrystallization grains, as seen in Fig. 7a and Fig. 7b. Fig. 8a shows that a large number of dislocations are stored in the grain interior of the Cu-1%Zr alloy deformed at 550°C with 0.1 s^{-1} strain rate. The dispersed secondary phases

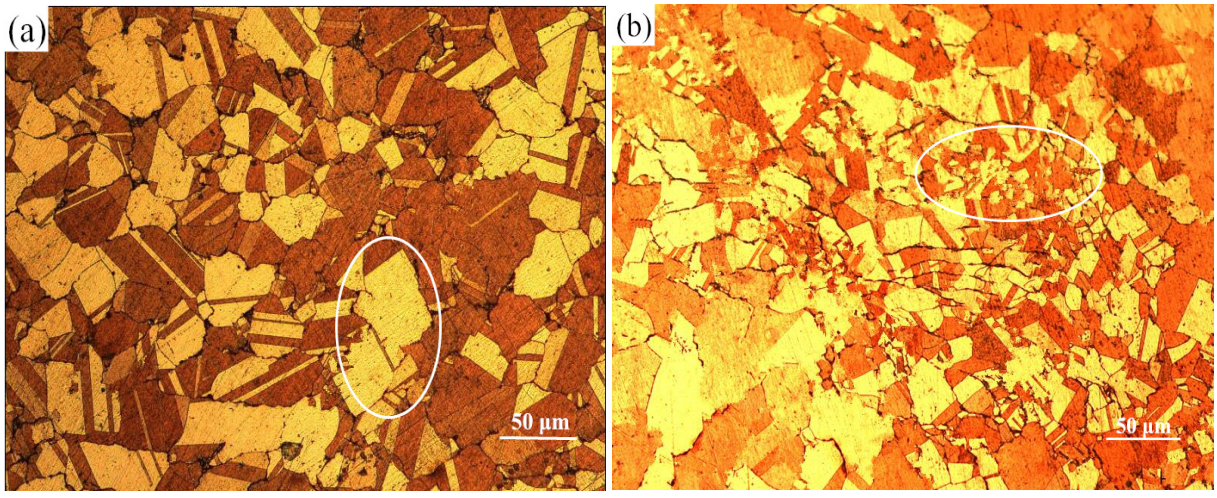

Fig. 6. Microstructure of: Cu-Zr(a) and Cu-1%Zr-0.15%Y(b) alloys after solution treatment at 900°C for 1 h

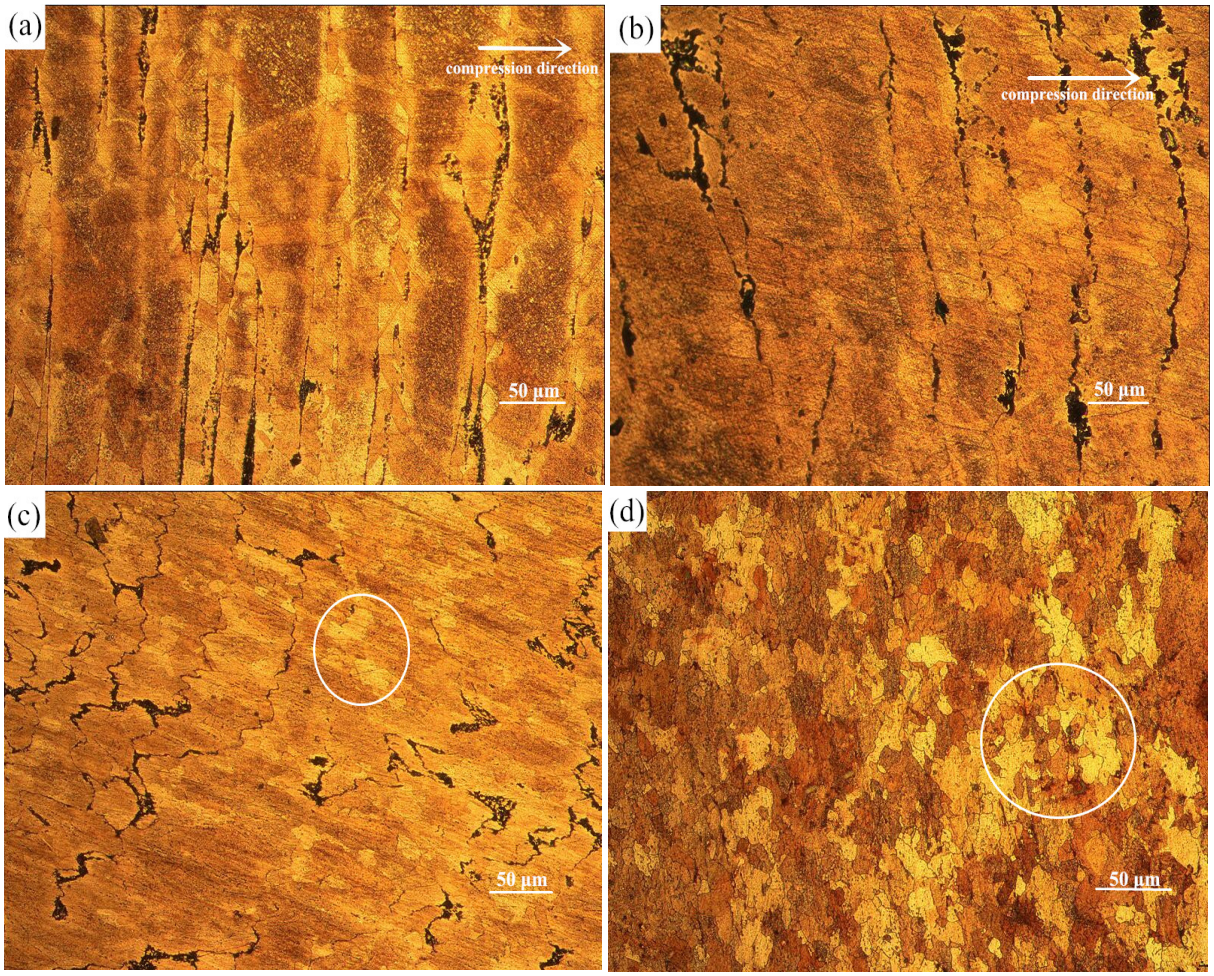

Fig. 7. Optical micrographs of the Cu-1%Zr(a,c) and Cu-1%Zr-0.15%Y(b,d) alloys hot deformed at 0.1 s^{-1} strain rate and different temperatures: (a) 550°C; (b) 550°C; (c) 850°C; (d) 850°C

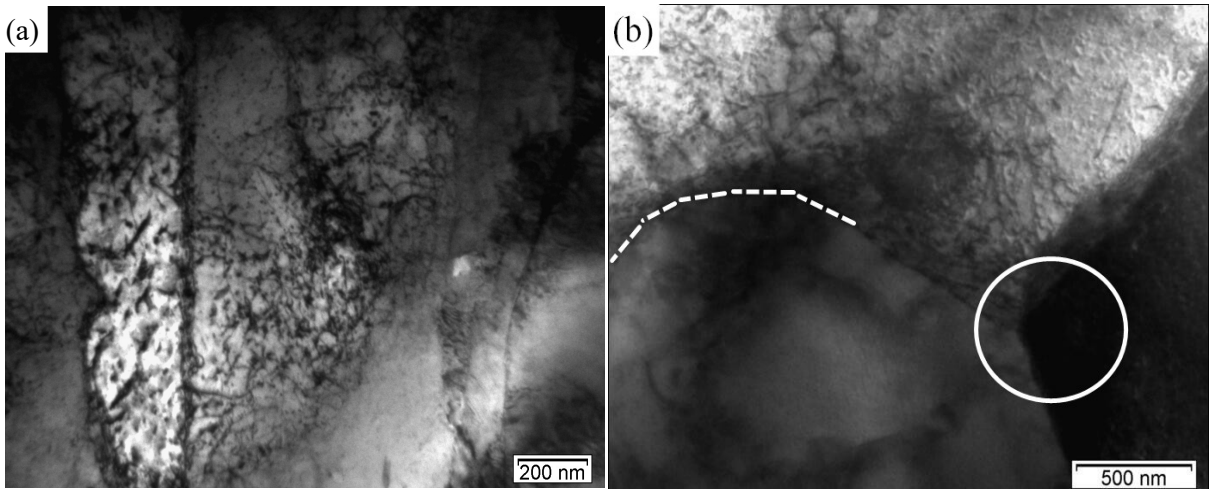

Fig. 8. TEM micrographs of the Cu-1%Zr alloy deformed at 0.1 s^{-1} strain rate and different temperatures: (a) 550°C; (b) 850°C

in the crystal and the secondary phases at the grain boundaries are obviously hinder dislocation and grain boundary movements. Surface tension leads to grain boundary protrusion into a circular arc shape, as seen in Fig. 8b. Nearly 120° grain boundaries show that sub-grain has begun to grow and merge, which is an obvious characteristic of dynamic recrystallization [24].

It can be seen from the ellipse marked by Fig. 7c and Fig. 7d, Cu-1%Zr alloy has less dynamic recrystallization grains, while Cu-1%Zr-0.15%Y alloy has more dynamic recrystallization grains. Under the same conditions, the addition of rare earth Y can contribute to the occurrence of dynamic recrystallization. The original grain size and the dispersed secondary phases are

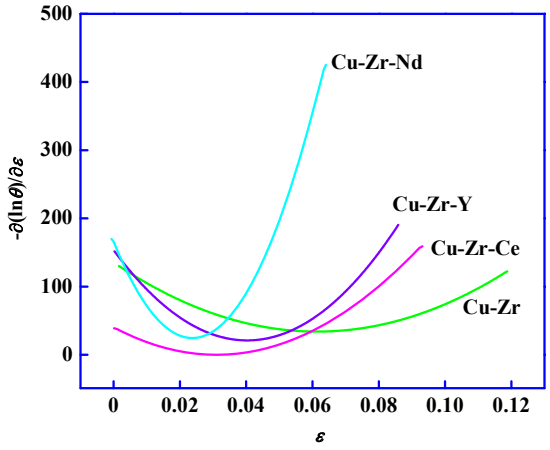

Fig. 9. Relationship between $\dot{\varepsilon}$ and ε for Cu-1%Zr(-0.15%RE) alloys under 900°C, 0.001 s^{-1}

important factors affecting dynamic recrystallization. The addition of Y has an obvious effect on the Cu-1%Zr grain refinement. The high density of very fine, semi-coherent Zr-rich particles effectively retard both dynamic recovery as well as grain boundary migration during dynamic recrystallization. Observed grain refinement for Cu-1%Zr-0.15%Y alloy result from the effect of increased stored energy that rises nucleation sites for DRX and reduce velocity of DRX grains growth in the presence of fine particles. Both fine Zr-rich particles as well as solid solution of Zr and Y in Cu matrix effectively retard dynamic structure restoration processes. On the other hand, dynamic recrystallization occurs at the beginning of a corresponding critical strain point. Theta-parameter is the derivative differential of stress in strain, $\theta = \partial\sigma/\partial\varepsilon$. The lowest point of curves are dynamic recrystallization critical strain point, as shown in Fig. 9. With the addition of rare earth, the critical strain points of dynamic recrystallization have been advanced. Therefore, the addition of rare earth Y can promote the occurrence of dynamic recrystallization.

4. Discussion

We found $Cu_{10}Zr_7$ in the experiment. There are many different opinions about the types of precipitates. Mu et al. [25] believe that the Cu-Cr-Zr-Mg-RE alloy has a zirconium-rich phase at 450°C. Su et al. [26] think precipitated phase is Cu_5Zr in the Cu-Cr-Zr alloy at 500°C aged for 30 min. Xie et al. [27] believe that Cu_4Zr precipitates are nucleated preferentially at the pre-nucleated Cr-rich particles in the Cu-Cr-Zr-Sn alloy, being semi-coherent with the matrix. Kawakatsu et al. [28] hold that Zr-rich precipitates in Cu-Cr-Zr are Cu_3Zr type. Deng et al. [29] believe that Cu-0.1%Zr alloy prepared by prepared by powder metallurgy method result in precipitation of Cu_2Zr particles during solid solution and aging treatment. Huang et al. [30] analyze the microstructure of Cu-0.31Cr-0.21Zr and the precipitated phase is considered as $Cu_{51}Zr_{14}$. Saitoh et al. [31] studied the microstructure formed by the eutectic reaction of Cu-Zr alloy with a Zr concentration of 12.3 mass % and the precipitated phase is considered as Cu_9Zr_2. The precipitated phase is $Cu_{10}Zr_7$ and its eutectic temperature is 895°C [28], while the solid solution treatment temperature is 900°C. The solution temperature and eutectic temperature are almost the same and higher Zr content addition results in $Cu_{10}Zr_7$ precipitation.

5. Conclusions

The Cu-1%Zr and Cu-1%Zr-0.15%Y alloys have similar hot compression deformation features. Typical characteristics of dynamic recovery occur at 550-750°C deformation temperature, while dynamic recrystallization operate at deformation temperature 850-900°C. High Zr content and the addition of Y significantly improve Cu-1%Zr alloy hot deformation activation energy. Compared with hot deformation activation energy of pure copper, hot deformation activation energy of the Cu-1%Zr and Cu-1%Zr-0.15%Y alloys is increased by 54% and 81%, respectively. Zr addition has solid solution strengthening effect, impeding dislocation slip and climb. The atomic radius of Cu and the atomic radius of Y are dramatically different and Y has an effect of removing impurities and deoxygenating, which make hot deformation activation energy of the Cu-1%Zr alloy increase by 18% with the addition of Y. The addition of Y refines the grain size, advances the dynamic recrystallization critical strain point and promotes the occurrence of dynamic recrystallization.

Acknowledgments

This work was supported by the National Natural Science Foundation of China (51101052) and the Science and Technology Innovation Talents in Universities of the Henan Province (14IRTSTHN007).

REFERENCES

[1] J.H. Su, Q.M. Dong, P. Liu, Mater. Sci. Eng. A **392** (1-2), 422-426 (2005).
[2] Y. Zhang, R.Q. Li, Q.Q. Xu, B.H. Tian, Y. Liu, P. Liu, X.H. Chen, The Chinese Journal of Nonferrous Metals **24** (3), 745-751 (2014).
[3] D.M. Zhao, Q.M. Dong, P. Liu, B.X. Kang, J.L. Huang, Z.H. Jin, Transactions of Nonferrous Metals Society of China **13** (2), 258-261 (2003).
[4] A. Chbihi , X. Sauvage, D. Blavette, Acta Mater. **60** (11), 4575-4585 (2012).
[5] J. Zou, L. Lu, D.P. Lu, K.M. Liu, Z.B. Chen, Q.J. Chai, J. Mater. Eng. Perform. **25** (3), 1062-1067 (2016).
[6] Q.Y. Dong, L.N. Shen, F. Cao, Y.L. Jia, K.J. Liao, M.P. Wang, J. Mater. Eng. Perform **24** (4), 1531-1539 (2015).
[7] Y. Zhang, B.H. Tian, A.A. Volinsky, H.L. Sun, Z. Chai, P. Liu, X.H. Chen, Y. Liu, J. Mater. Eng. Perform. **25** (4), 1336-1341 (2016).
[8] I. Shakhova, Z. Yanushkevich, A. Belyakov, R. Kaibyshev, Mater. Sci. Eng. A **606**, 380-389 (2014).

[9] M.F. Chen, C. You, Journal of Tianjin Institute of Technology **14**, 42-46 (1998).
[10] J.H. Su, F.Z. Ren, B.H. Tian, P. Liu, Q.M. Dong, J. Mater. Sci. Technol. **25** (2), 230-232 (2009).
[11] H.F. Xie, X.J. Mi, G.J. Huang, X.Q. Yin, Y.F. Li, B.D. Gao, Rare Metals, **35** (3), 458-462 (2011).
[12] F.X. Yu, J.Y. Cheng, B. Shen, The Chinese Journal of Nonferrous Metals **23** (12), 3360-3366 (2013).
[13] W. Wang, R.G. Li, C.L. Zou, Z.N. Chen, W. Wen, T.M. Wang, G.M. Yin, Mater. Des. **92**, 135-142 (2016).
[14] L. Jiang, F. Jiang, C. Dai, X. Wang, W. Zong, The Chinese Journal of Nonferrous Metals **20** (5), 878-884 (2010).
[15] Y. Zhang, Z. Chai, A.A. Volinsky, B.H. Tian, H.L. Sun, P. Liu, Y. Liu, Mater. Sci. Eng. A **662**, 320-329 (2016).
[16] G.X. Hu, X. Cai, Y.H. Rong, Fundamentals of Materials Science, Shang Hai (2009).
[17] C.M. Sellars, W.J. McTegart, Acta Mater. **14** (9), 1136-1138 (1966).
[18] M. Morakabatia, S.H. Kheirandish, M. Aboutalebi, A. Karimi Taheri, S.M. Abbasi, J. Alloys Compd **499** (1), 57-62 (2010).
[19] A. Momeni, K. Dehghani, Mater. Sci. Eng. A **527** (21-22), 5467-5473 (2010).
[20] Y. Deng, Z.M. Yin, J.W. Huang, Mater. Sci. Eng. A **528** (3), 1780-1786 (2011).
[21] C. Zener, J.H. Hollomon, J. Appl. Phys. **15** (1), 22-32 (1944).
[22] R.L. Zhao, Y. Liu, B.H. Tian, X.W. Zhang, Y. Zhang, Heat Treatment of Metals **36** (8), 17-20 (2011).
[23] J.L. Glimois, P. Forey, J. Feron, C. Becle, Journal of The Less--Common Metals **78** (1), 45-50 (1981).
[24] S.L. Yang, J. Shen, X.D. Yan, X.W. Li, B.J. Sun, F. Zhang, Transactions of Nonferrous Metals Society of China **25**, 2083-2090 (2015).
[25] S.G. Mu, F.A. Guo, Y.Q. Tang, X.M. Cao, M.T., Mater. Sci. Eng. A **475** (1-2), 235-240 (2008).
[26] J.H. Su, P. Liu, Q.M. Dong, H.J. Liu, F.Z. Ren, B.H. Tian, Transactions of Materials and Heat Treatment **26** (6), 62-65 (2005).
[27] H.F. Xie, X.J. Mi, G.J. Huang, B.D. Gao, X.Q. Yin, Y.F. Li, Rare Metal Materials and Engineering **41** (9), 1549-1554 (2012).
[28] I. Kawakatsu, H. Suzuki, H. Kitano, J. Jpn. Inst. Met. **31**, 1253-1257 (1967).
[29] J.Q. Deng, Y.C. Wu, F.W. Yu, D.G. Wang, Rare Metal Materials and Engineering **38** (4), 205-208 (2009).
[30] F.X. Huang, J.S. Ma, H.L. Ning, Scripta Materialia **48** (1), 97-102 (2003).
[31] M. Saitoh, M. Kajihara, Y. Tomioka, Mater. Sci. Eng. A **318** (1-2), 87-93 (2001).